DOI: 10.1002/cbic.201100485

Mechanistic Insight into the Catalytic Activity of ββα-Metallonucleases from Computer Simulations: *Vibrio vulnificus* Periplasmic Nuclease as a Test Case

Juan A. Bueren-Calabuig,[a] Claire Coderch,[a] Eva Rico,[b] Antonio Jiménez-Ruiz,[b] and Federico Gago*[a]

Using information from wild-type and mutant *Vibrio vulnificus* nuclease (Vvn) and I-PpoI homing endonuclease co-crystallized with different oligodeoxynucleotides, we have built the complex of Vvn with a DNA octamer and carried out a series of simulations to dissect the catalytic mechanism of this metallonuclease in a stepwise fashion. The distinct roles played in the reaction by individual active site residues, the metal cation and water molecules have been clarified by using a combination of classical molecular dynamics simulations and quantum mechanical calculations. Our results strongly support the most parsimonious catalytic mechanism, namely one in which a single water molecule from bulk solvent is used to cleave the phosphodiester bond and protonate the 3′-hydroxylate leaving group.

Introduction

Sugar nonspecific endonucleases belong to a family of enzymes that are able to cleave single- and double-stranded (ds) DNA and/or RNA molecules with little or no sequence specificity.[1] They have been identified in several organisms and the three-dimensional structures of some of them have been solved by X-ray crystallography and deposited in the Protein Data Bank (PDB).[2] The best studied representatives are *Serratia marcescens* nuclease (Smn),[3,4] nuclease A from *Anabaena* sp. (NucA),[5] and the periplasmic nuclease from *Vibrio vulnificus* (Vvn).[6,7] From a structural viewpoint, all of these enzymes belong to the ββα-metal superfamily of nucleases that use just one divalent metal ion[8] to bring the reactant species into close proximity and catalyze the reaction.[9] In this respect, the cation, usually but not exclusively, magnesium, has been proposed to act as a Lewis acid to activate a bound nucleophile (e.g., by promoting ionization of water to a more reactive hydroxide) and/or to stabilize the negative charge on the pentacoordinate trigonal bipyramidal transition state (TS) and the 3′-hydroxylate leaving group.

The common structural core of these metallonucleases is made up of two antiparallel β-sheets and one α-helix that contains an essential and strictly conserved asparagine residue, the carboxamide oxygen of which is used to coordinate the metal ion, hence the family name (Figure S1 in the Supporting Information). A signature motif in the first β-strand is a DRGH sequence, where H is the active site histidine,[1] although in Vvn it is replaced by EWEH,[6] with the peculiarity that the side-chain carboxylate of the second glutamate (E) residue is also involved in metal binding (Mg^{2+} or Ca^{2+}). The finding that site-directed mutation of the common histidine in this motif leads to a dramatic decrease in endonuclease activity has demonstrated the critical role of this residue in catalysis, most likely as a general base that activates the water molecule responsible for internucleotide phosphodiester cleavage.[6] Thus, following abstraction of a proton from the water molecule, the resulting hydroxide anion would initiate an in-line nucleophilic attack on the phosphorus atom leading to cleavage of the O3′–P bond. The two final products of the reaction are a nucleic acid strand with a 5′-phosphorylated end and another one with a terminal 3′ hydroxyl group. Nonetheless, there appears to be no consensus yet as to whether the attacking water is in direct coordination with Mg^{2+} or is a free solvent molecule.[3,10–12]

Equally debated is the origin of the proton that needs to be donated to the 3′-hydroxylate leaving group. In this respect, either a general acid (e.g., Glu127 in Smn[4,13] or Glu163 in NucA[14]) or a second water molecule from the inner coordination sphere of the metal ion have been advocated.[6,13,15] The large number and diversity of the proposed mechanisms attest to the fact that the atomic details of some steps of the reaction are still unclear despite the relative wealth of crystallographic structures, albeit in the absence of DNA.[1] An exception is Vvn, for which two different crystals were solved some years ago, one containing the active form of the metallonuclease in the absence of DNA and another containing two His80Ala mutant enzymes with Ca^{2+} in the active site forming a complex with two DNA octanucleotides, one intact and one cleaved.[6,15] More recently, the structure of another complex of Vvn in complex with a 16 bp DNA in the absence of metal ions was solved.[7] However, none of these enzyme–substrate (E–S)

[a] *J. A. Bueren-Calabuig, C. Coderch, Prof. F. Gago*
Department of Pharmacology, Universidad de Alcalá
28871 Alcalá de Henares, Madrid (Spain)
E-mail: federico.gago@uah.es

[b] *Dr. E. Rico, Prof. A. Jiménez-Ruiz*
Department of Biochemistry and Molecular Biology
Universidad de Alcalá, 28871 Alcalá de Henares, Madrid (Spain)

Supporting information for this article is available on the WWW under http://dx.doi.org/10.1002/cbic.201100485.

 © 2011 Wiley-VCH Verlag GmbH & Co. KGaA, Weinheim

or enzyme–product (E–P) complexes provides an answer to the above-mentioned questions principally because no water molecule is properly positioned for attack and because the DNA phosphate backbone adopts a standard conformation that is unsuitable for the reaction to proceed.

The active site of Smn, NucA and Vvn is also very similar to those of apoptotic endonuclease G from *Drosophila melanogaster* (Dm-endoG),[16] the His-Cys box homing endonuclease, I-PpoI, from the slime mould *Physarum polycephalum*,[17–19] the DNA-entry nuclease EndA from *Streptococcus pneumoniae*,[20] and a recently identified endonuclease from the protozoan parasite *Leishmania infantum* (Li-endoG)[21] (Figure S1 in the Supporting Information). Moreover, cleavage experiments with deoxythymidine 3′,5′-bis-(*p*-nitrophenylphosphate) as an artificial minimal substrate have indeed shown that Smn, NucA and I-PpoI follow the same mechanism of phosphodiester bond hydrolysis.[11,13,22] Of particular interest for our purposes is I-PpoI because its DNA-bound structure has been determined as three distinct species on the reaction pathway, including two trapped E–S complexes that clearly display the hydrolytic water in the vicinity of the strictly conserved catalytic histidine (His98) and one E–P complex with the same ds-DNA 21-mer cleaved in one strand.[17,18] Of note, in the complex containing an inactive His98Ala mutant, the Mg^{2+} ion is coordinated by the side-chain carboxamide oxygen of the conserved asparagine (Asn119), three water oxygen atoms and two phosphate oxygen atoms from the DNA substrate: the bridging O3′ and the nonbridging OP1. This information is particularly noteworthy as it clearly indicates that the phosphate backbone has to undergo a well-defined conformational change at the site of cleavage.

Given that advances in computational power and maturity of force fields for nucleic acids and proteins allow us to fill in some of the missing pieces that experimental techniques cannot always provide,[23] it is currently possible to simulate the course of an enzymatic reaction stepwise, starting with formation of the Michaelis–Menten protein–substrate complex and ending up with product release after resolution of the TS.[24,25] In order to shed light on the catalytic mechanism of Vvn, we decided to use a combination of molecular dynamics (MD) and quantum mechanics/molecular mechanics (QM/MM) calculations on the active form of Vvn in complex with a ds-DNA octamer. The main advantage of a hybrid approach involving MD and QM for the solvated DNA–protein complex over studies that focus on simplified model systems is that bond making and breaking are possible in a dynamic context and also that reorganization of active site residues and water molecules is realistically allowed through the whole procedure. Our results strongly support the most parsimonious catalytic mechanism, namely one in which there is no need to invoke more than a single water molecule to accomplish the complete reaction, that is, cleavage of the phosphodiester bond and protonation of the leaving hydroxylate.

Results and Discussion

Initial Vvn–DNA complex

The initial model used in our simulations represents a Michaelis–Menten complex of the active form of Vvn, that is, a fully competent enzyme containing the catalytic His80 and Mg^{2+} as the metal cation, in complex with a ds-DNA octamer in which the phosphodiester bond to be cleaved adopts a suitable conformation for the nucleophilic attack, as found in the crystal structure of a I-PpoI–DNA complex (PDB ID: 1CYQ).[17] Consequently, this structure, which still lacks a properly positioned hydrolytic water, differs from those obtained for Vvn by using X-ray crystallography, which show either an active enzyme in the absence of DNA (PDB ID: 1OUO) or a mutant His80Ala enzyme in complex with either an octanucleotide and bound Ca^{2+} (PDB ID: 1OUP) or a 15-mer in the absence of any cation (PDB ID: 2IVK). In the latter two cases, the DNA phosphate backbone adopts a standard B-type conformation.[6,7] In our model, on the other hand, the nonbridging OP1(Gua_{15}) and the bridging O3′(Ade_{14}) complete the octahedral coordination of Mg^{2+} in addition to Oε1(Glu79), Oδ(Asn127), and the oxygen atoms of two water molecules that are present in the apo form crystal of Vvn. According to this geometrical disposition, the O3′—P phosphodiester bond to be cleaved belongs to the phosphate linking Ade_{14} to Gua_{15} in the second DNA strand, that is, the underlined step in d(TCTTAAGA)–d(TCTTAAGA). Importantly, by adopting this backbone conformation, binding of the DNA strand to Vvn is further stabilized by two additional hydrogen bonds: one between O5′(Gua_{15}) and Nδ(Asn127), and another between OP2(Gua_{15}) and the guanidinium of Arg99, which is fixed in position by ion pair formation with the carboxylate of Glu113 and appears to be bound to the terminal 5′-phosphate in the E–P complex.[6]

The side chain of the catalytically essential Asn127 is thus remarkably fixed for binding to O5′ through Nδ and for bringing the negatively charged phosphate into a proper conformation for attack because, in addition to its backbone carbonyl oxygen being coordinated to Mg^{2+}, Asn127 simultaneously engages its Nδ in a hydrogen bond to the carboxylate of Glu77, which is in turn stabilized by the guanidinium of Arg72 (Figure 1). On the other hand, the imidazole ring of His80, the residue responsible for water molecule activation (i.e., proton abstraction by Nδ) is also relatively fixed and made more basic because of a hydrogen bond between its Nε and the backbone carbonyl oxygen of Glu113[6] (positionally equivalent to Cys105 in I-PpoI[17] and Asn106 in Smn[3,4]).

Incidentally, another stable hydrogen bond that was observed in our simulation, as a consequence of the sugar–phosphate rearrangement and mutual DNA–protein adaptation, was that established between NH1(Arg72) and N3(Ade_{14}). This interaction could account for the scarcity of adenines at sites cleaved by Vvn despite its little sequence preference in DNA.[7] The guanidinium of Arg72 is held in position to face the DNA minor groove by means of a buttressing interaction with the carboxylate of Glu77 (the first E in the EWEH motif), as also seen in the Vvn–DNA crystal structures. However, the closer in-

 © 2011 Wiley-VCH Verlag GmbH & Co. KGaA, Weinheim

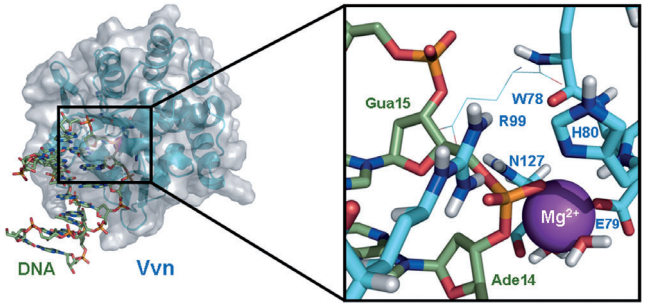

Figure 1. Structural model and close-up view of Vvn (cyan) in complex with DNA (green) in a near-attack reactive conformation. The active site Mg^{2+} is coordinated by two water molecules, O=C(Asn127), a carboxylate oxygen from Glu79, the nonbridging oxygen OP1(Gua_{15}) and O3′(Ade_{14}). The Vvn–DNA complex is stabilized in this region by an electrostatic interaction between the guanidinium of Arg99 and the scissile phosphate and also by a hydrogen bond that is established between Nδ(Asn127) and O5′(Gua_{15}).

teraction between Arg72 and the DNA base is not so apparent possibly because the side chain of this residue faces a G:C base pair in PDB entries 2IVK and 1OUP and, consequently, the presence of an exocyclic amino group in the minor groove decreases the goodness of this interaction with either N3 of guanine or O2 of cytosine.

Activation of a water molecule by His80

After 3 ns of MD equilibration of the Vvn–DNA complex in aqueous solution, a water molecule from the bulk solvent entered the active site and remained fixed at a location suitable for the nucleophilic attack to proceed. In fact, an average OW(water)–P(Gua_{15}) distance of $\leq$4.0 Å and an average O3′(Ade_{14})–P(Gua_{15})–OW(water) angle of approximately 176° suggested an ideal position for in-line attack on the O3′–P bond. Furthermore, the distance between the same OW atom in this location and both Nδ(His80) and O=C(Trp78) was also $\leq$4.0 Å. Therefore, this water molecule was unbiasedly trapped for the rest of the simulation, with one of its oxygen's lone pairs properly oriented for attack, even though its protons (HW) swapped their interactions with the two hydrogen bond acceptor atoms of these two amino acids (Figure 2). When we compared this water location with that of the hydrolytic water in the I-PpoI–DNA complexes, they were found to be perfectly superimposable.

The α/γ torsion angles of the cleavable phosphate group linking Ade_{14} and Gua_{15} remained mostly constant in a *trans*/*trans* (*t*/*t*) conformation during the first 2 ns of simulation but then changed to negative and positive *anticlinal* (*ac*−/*ac*+) and later to positive and negative *gauche* (*g*+/*g*−; Figure 2B). After these fast crankshaft motions of the DNA sugar–phosphate backbone, the α/γ torsionals returned to their original *t*/*t* configuration for the rest of the simulation. During all this time, Nδ(Asn127) remained hydrogen bonded to O5′(Gua_{15}) except for the period when the α/γ torsion angles were in the *ac*−/*ac*+ DNA conformation. Interestingly, the return to the catalytically relevant *t*/*t* backbone configuration after the initial fluctuations, was concomitant with the approach and proper

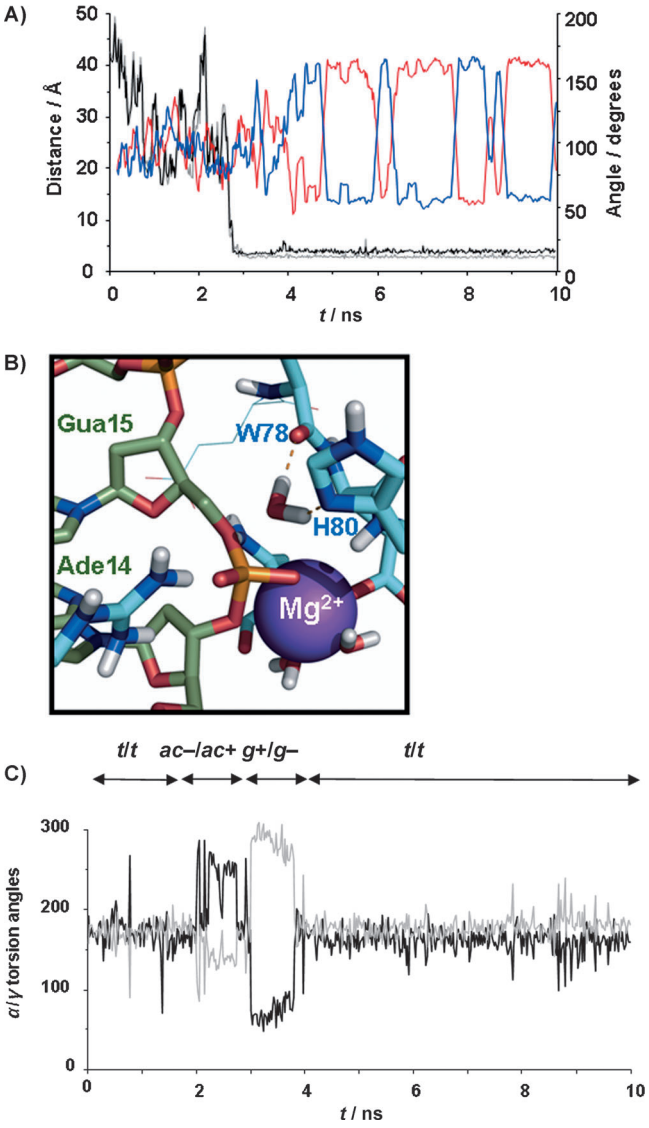

Figure 2. A) Time evolution of the distances between the oxygen (OW) of the nucleophilic water molecule and both the phosphorus atom (black) and Nδ(His80) (grey). The angle formed by each water hydrogen (HW1 and HW2, red and blue), the water oxygen (OW), and Nδ(His80) is also represented in the secondary vertical axis. B) Representative snapshot from our simulation of the active site of Vvn in its complex with the DNA octamer showing this water molecule correctly hydrogen bonded to O=C(Trp78) and Nδ(His80) and suitably positioned for the in-line attack. C) Time evolution of the α and γ backbone torsion angles of Gua_{15} (*t*, *ac*, and *g* stand for *trans*, *anticlinal*, and *gauche*, respectively). Note that the stability achieved after approximately 4 ns is concomitant with the monotonic OW–P distance displayed in Figure 2A.

positioning of the catalytic water molecule and fixation via hydrogen bonding to both Nδ(His80) and O=C(Trp78).

Moreover, when we docked deoxythymidine 3′,5′-bis-(*p*-nitrophenylphosphate) into the active site of Vvn by using an automated force-field-based method that allows for ligand flexibility,[26] the best-scoring pose adopted the same *t*/*t* conformation for the α/γ torsion angles of the cleavable phosphate (Figure S2 in the Supporting Information). This artificial minimal substrate is cleaved by Smn,[11,13] NucA[14] and I-PpoI[22] at its 5′ end, albeit at a much lower rate than DNA or RNA, to

 © 2011 Wiley-VCH Verlag GmbH & Co. KGaA, Weinheim

produce nitrophenol and deoxythymidine 3′-(*p*-nitrophenylphosphate) 5′-phosphate. The scissile bond for these metallonucleases is, therefore, different from that attacked by staphylococcal nuclease (O5′–P) or pancreatic DNase I (O–P bond linking the other *p*-nitrophenol moiety to the 3′-phosphate on thymidine),[1] in agreement with the fact that Smn, NucA, I-PpoI and, by extension, Vvn need at least a second phosphate group to be present 3′ to the bond to be cleaved. This has also been shown for Smn by using oligodeoxynucleotides substituted by a single phosphorothioate group.[11] In the case of Vvn, this second phosphate hydrogen bonds to the backbone NH of Trp85, the side-chain indole nitrogen of which, together with that of Trp94, is engaged in yet another hydrogen bond with the following phosphate in the oligonucleotide strand. On the other side of the cleavable bond, it is the side chains of Arg75 and Lys28 that establish hydrogen bonds with the O5′ and OP2 of another nucleotide in the same strand, as well as Lys54 with the next phosphate.[6,15] Thus, in common with Smn,[11] a minimum of five phosphate groups would appear to be necessary for high-affinity DNA binding and moderately good cleavage activity by Vvn.

The simulated trajectory of the Vvn–DNA complex showed that the short hydrogen bond between Nε(His80) and O=C(Glu113), which is present in the crystal structure[6] and thought to make the imidazole a stronger base to facilitate water deprotonation, was also maintained. To proceed with the cleavage reaction, therefore, we subjected the active site region to QM treatment during the course of the MD simulation and defined two double reaction coordinates for simultaneously shortening the HW–Nε and OW–P distances and stretching the HW–OW and O3′–P bonds, as explained in the Computational Methods.

Nucleophilic attack and intermediate product generation

As a result of the QM reaction coordinate: 1) a hydroxide was generated, in situ, that attacked the phosphodiester bond, 2) an imidazolium was formed on the side chain of His80, and 3) the negative charge on the pentacoordinate trigonal bipyramidal TS was stabilized by Mg^{2+} (coordinated to OP1 and O3′) and the guanidinium side chain of Arg99 (forming an ion pair with OP2; Figure S3 in the Supporting Information). This latter interaction has been previously observed only in the E–P complexes solved by X-ray crystallography.[6,15] Subsequent collapse of the TS yielded the intermediate products of this first part of the reaction, namely a 5′-phosphorylated dinucleotide, d(GA), and a d(TCTTAA) hexanucleotide with a terminal 3′-hydroxylate, both of them still hydrogen bonded to the intact complementary strand, d(TCTTAAGA), (movie SM1 in the Supporting Information).

An unrestrained MD simulation of this updated system configuration showed the immediate loss of the original hydrogen bond between the protonated Nδ(His80$^+$) and OW (now belonging to the new terminal phosphate) and formation of a new hydrogen bond between the imidazolium Nδ and OP2 of the same phosphate group. This latter interaction was maintained for the remaining part of the 10 ns simulation except

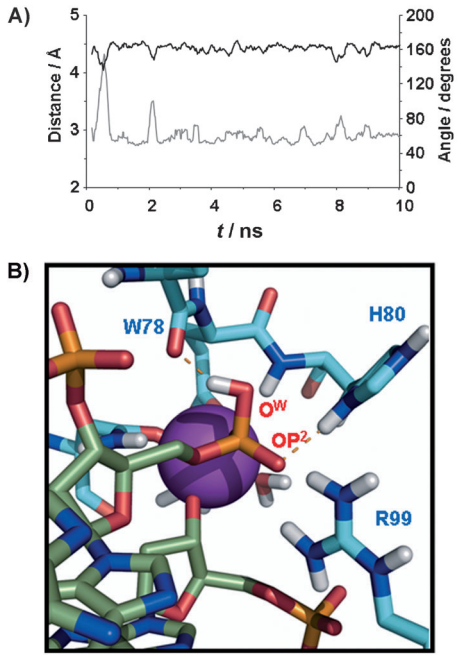

Figure 3. A) Time evolution of: 1) the distance (grey) between the phosphate nonbridging oxygen OP2 and Nδ(His80), and 2) the angle (black) between OP2, HNδ(His80) and Nδ(His80). B) The HNδ(His80) proton (originally HW) is proposed to be transferred to the OP2 phosphate on its way to the O3′ hydroxylate.

for brief exchanges with OW (Figure 3). At this point, the active site architecture reproduced very accurately the overall geometry found in the crystallographic E–P complex containing the His80Ala mutant Vvn (PDB ID: 1OUP) but showed an improved hydrogen-bonding interaction between the terminal phosphate O5′ and Nδ(Asn127). On the other hand, the hydrogen bond between OP2 and NH2(Arg99) might ensure that this product does not evolve backwards to favour the reverse reaction[6] (see below). The equivalent residue in Smn is Arg57, the mutation of which to Ala has been shown to decrease the activity of the wild-type enzyme by $>99\,\%$.[11]

Deprotonation of His80

In view of the stability of the hydrogen bond established between OP2 and Nδ(His80$^+$), we reasoned that it was perfectly feasible for the proton on Nδ to be transferred to this negatively charged phosphate oxygen. A QM reaction coordinate was employed for this purpose (Figure S4 in the Supporting Information) and the new connectivity was used to simulate the resulting system configuration for a further 10 ns. Interestingly, in this new simulation, the two hydroxyls in the terminal phosphate rotated about their O–P bonds after approximately 3 ns and exchanged hydrogen bond acceptors through water-mediated interactions (Figure 4). Thus, the original hydrogen bond between Nδ(His80$^+$) and OP2 was lost and replaced with a new one between OP2 and the negatively charged, Mg^{2+}-bound O3′. Reciprocally, Nδ(His80) became engaged in a hydrogen bond with the phosphate OW after losing its close

 © 2011 Wiley-VCH Verlag GmbH & Co. KGaA, Weinheim

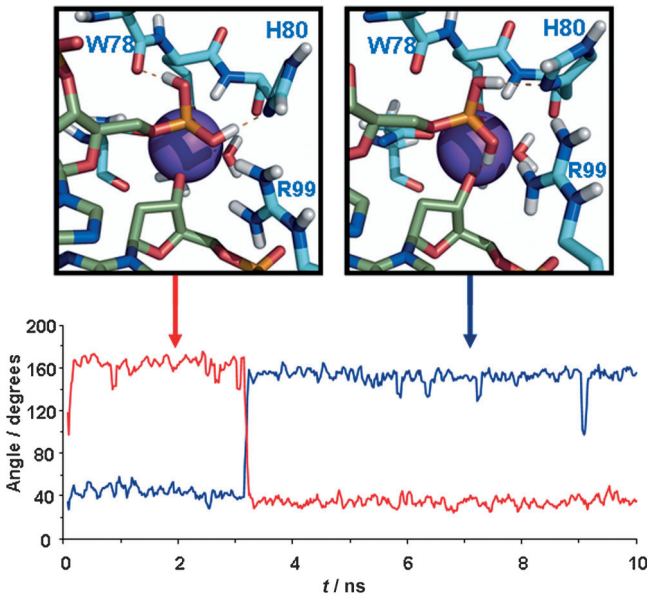

Figure 4. Swapping of hydrogen bonding partners for the newly created terminal phosphate bearing two hydroxyl groups on the phosphorus atom after transfer of the proton from Nδ(His80) to OP2: the OP2–HW···Nδ(His80) hydrogen bond (red) is broken whereas a new OP2–HW···O3′ hydrogen bond (blue) is formed.

interaction with O=C(Trp78), which in turn became solvated by water.

Protonation of the leaving group

In this new setting it became apparent that OP2, still hydrogen bonded to NH1(Arg99), was the most likely proton donor to $O3'^{(-)}$ (Figure 4). This shuttle mechanism would imply that the leaving group can be protonated by a hydrogen originating from the same water molecule that initiated the nucleophilic attack. The QM reaction coordinate showed the feasibility of this proposal (Figure S5 in the Supporting Information) and rendered: 1) a neutral hydroxyl, the oxygen of which was still coordinating the Mg^{2+}, and 2) a terminal 5′-phosphate bearing a charge of −1 (Figure 5). Consequently, there appears to be neither structural support nor any need to invoke the unlikely deprotonation[9,27] by the metal cation of a second water molecule, as postulated in several unproven mechanistic proposals. On the one hand, $O3'^{(-)}$ itself is coordinating the metal, on the same plane as the two liganded water molecules; on the other hand, the only other water close to $O3'^{(-)}$ belongs to the second solvation shell of Mg^{2+} and is hydrogen bonded to $OP2(Gua_{15})$ and NH1(Arg99).

Exit of the products from the active site

During the MD simulation of the system containing the cleaved DNA strand: 1) both $OP1(Gua_{15})$ and $O3'(Ade_{14})$ retained their coordination to the Mg^{2+} cation, and 2) the backbone O=C(Asn127) and carboxamide Nδ(Asn127) remained hydrogen bonded to O3′ (acting as a donor) and O5′ (acting as an acceptor), respectively. On the contrary, the guanidinium of

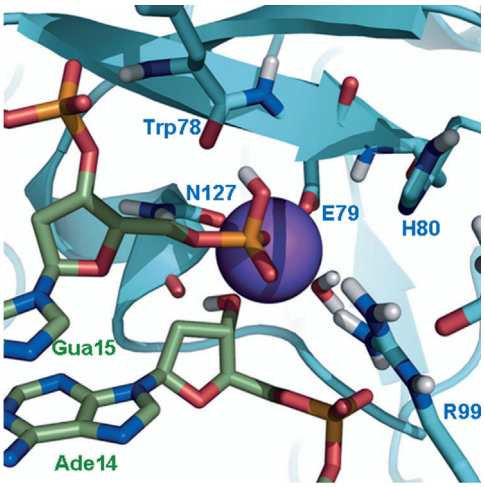

Figure 5. Detail of the active site of Vvn immediately after formation of the final products of the cleavage reaction. Note the singly protonated terminal 5′-phosphate, the free 3′-hydroxyl and the neutral imidazole in His80.

Arg99 started to weaken its interaction with the just created terminal 5′-phosphate on Gua_{15}, which started to become fully solvated, but maintained its hydrogen bond with the phosphate group linking Ade_{14} to Ade_{13}. Although much longer simulation times could be expected to reproduce the separation of the DNA containing the cleaved strand from the Mg^{2+}-bound protein as a result of continued solvation of the binding partners, we did not pursue this issue any further after 25 ns. Instead, we made use of a normal mode analysis (NMA) to study the large-amplitude protein motions that most likely contribute to vacation of the active site and product release. Our rationale was that whereas a 10 ns MD simulation has been shown to be long enough for an enzymatic protein to visit several crystallographic conformations,[28] other larger-scale motions possibly related to catalysis occur on the microsecond-to-millisecond timescale. Fortunately, experimentally observed conformational changes connecting open and closed states, which usually limit the overall catalytic rate of many enzymes, are often correlated with low-frequency normal modes[23,25] that can be inexpensively calculated.[29] For Vvn, we found that the first nontrivial lowest-frequency mode (upon removal of the six rigid motions of rotation and translation) represented a clasping motion involving two domains on both sides of the DNA-binding cleft (movie SM2 in the Supporting Information). Vvn can then be likened to a hand that is able to grasp an incoming DNA when closed, and to release a cleaved oligonucleotide when open. For the latter to occur, Arg72 (supported by Glu77) and Arg75 in one domain would be in charge of pulling the nucleotide containing the 5′-phosphate out of the active site, whereas Arg99 (supported by Glu113) in the other domain would evacuate the strand containing the free 3′-hydroxyl by virtue of a strong electrostatic interaction with the preceding phosphate. This view is consistent with the finding that at the end of our 25 ns fully unrestrained MD simulation Arg99 started to lose its interaction with $O5'(Gua_{15})$ (>3.7 Å) whereas it maintained a short hydrogen bond with $O3'(Ade_{14})$.

 © 2011 Wiley-VCH Verlag GmbH & Co. KGaA, Weinheim

Conclusion

Although the active site architecture of several nonspecific ββα-metallonucleases and related enzymes is known in atomic detail, and despite the fact that site-directed mutagenesis experiments have shed light onto the critical residues involved in DNA cleavage, their full catalytic mechanism has remained elusive so far. The main uncertainties concern the origin of the hydrolytic water and the source of the hydrogen that protonates the leaving group. We thought that theoretical methods that combine QM and MM in a dynamic context could be of value in this respect, and chose the well-characterized Vvn as a representative example of this interesting class of nucleases.

Starting with a Vvn–DNA complex that was built by using crystallographic information from the structures of the complexes of wild-type and mutant Vvn and I-PpoI nuclease with different oligonucleotides, we carried out a series of simulations to dissect the catalytic mechanism of Vvn in a stepwise fashion. The stability of the DNA and protein conformations in the complex throughout the whole procedure was assessed by monitoring the root-mean-square deviation from the initial model (Figure S6 in the Supporting Information). The results obtained have allowed us to characterize the putative roles that individual active site residues play in the reaction path and have provided plausible answers to some long-standing issues. The principal findings (Figure 6) can be summarized as follows: 1) the imidazole of His80, aided by O=C(Glu113), functions as the general base that abstracts a proton from a water molecule and generates the hydroxide anion that then serves as the attacking nucleophile on the phosphorus atom; 2) this water molecule originates from the bulk solvent, and not from the hydration sphere of the metal cation, and is held in place by Nδ(His80) and O=C(Trp78); 3) proper positioning of this water is coupled to a sugar–phosphate rearrangement that is made possible by: i) coordination of Mg^{2+} with the nonbridging OP1 and the bridging O3′ oxygen atoms in the phosphate group to be cleaved, and ii) hydrogen bonding of O5′ to Nδ(Asn127); 4) attack of the in situ generated hydroxide is in-line with the O3′–P phosphodiester bond and the associative (S_N2) reaction proceeds without a covalent intermediate; 5) the pentacoordinate trigonal bipyramidal phosphorane-like TS is stabilized by Mg^{2+}, which is coordinated by OP1 and O3′, and by the guanidinium side chain of Arg99, which forms an ion pair with OP2; 6) an OP2-mediated proton shuttle from Nδ(His80) to the O3′ leaving group appears more probable than the abstraction of a proton from a second water molecule in the coordination sphere of Mg^{2+}, as previously proposed.

The catalytic mechanism that we have dissected for Vvn is likely to be shared by other members of the family and related ββα-metal nucleases that rely on the activation of a water molecule by the imidazole ring of a suitably positioned His to cleave both DNA and RNA in double- and single-stranded forms. The role of the only metal ion would be, on the one hand, to attract and stabilize the DNA substrate by forming a network of interactions with protein residues, water molecules and nucleotides that thereafter facilitates the positioning and activation of a water molecule for the nucleophilic attack and, on the other hand, to stabilize the TS of the reaction, which also interacts strongly with Arg99.

We are aware of the limitations of the semiempirical method that we have used, which was the only one currently implemented in the AMBER distribution that allowed us to study a molecular system containing both P atoms and a Mg^{2+} ion. For this reason we have not attempted to obtain the free energy profile of the reaction, which still needs to be done using a better Hamiltonian for the QM calculations. Nonetheless, the structural and geometrical characterization provides a plausible mechanism and will hopefully open new avenues for further theoretical and experimental research.

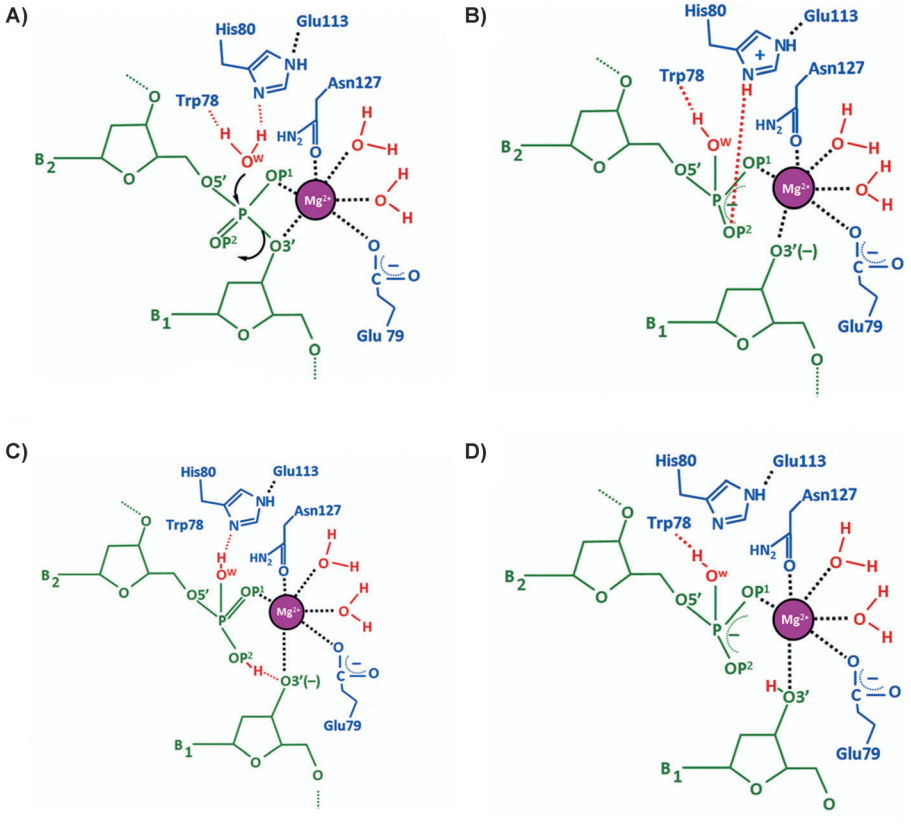

Figure 6. Full catalytic mechanism of Vvn in light of our computer simulation results. Note that the hydrogen bond between O5′(Gua_{15}) and Nδ(Asn127) has been omitted for clarity.

 © 2011 Wiley-VCH Verlag GmbH & Co. KGaA, Weinheim

Computational Methods

Construction of the Vvn–DNA complex: Since no structural data of the active form of Vvn in complex with DNA were available, a model was built by superimposing the ββα motif of wild-type, Mg^{2+}-bound Vvn (PDB ID: 1OUO) in the absence of DNA onto the ββα of the homing endonuclease I-PpoI in complex with a 21-mer (PDB ID: 1CYQ),[17] of which we kept only the central self-complementary d(TCTTAAGA)$_2$ octanucleotide. As a result, OP1(Gua$_{15}$) and O3′(Ade$_{14}$) from the DNA octamer occupied the same positions as two crystallographic water molecules in the unbound Vvn structure. The Mg^{2+} was then coordinated by these two phosphate oxygen atoms, Oδ1(Asn127), Oε1(Glu79), and two other water molecules. By superimposing the crystal structure of inactive, Ca^{2+}-bound Vvn complexed with DNA (PDB ID: 1OUP) over our construction, the most noticeable difference affected the conformation of the O3′–P–O5′–C5′(α)/O5′–C5′–C4′–C3′(γ) torsion angles of the cleavable phosphate.

Molecular dynamics simulations: The Vvn–DNA complex was immersed in a truncated octahedron of TIP3P water molecules[30] that extended 15 Å away from any solute atom. Incorporation of the appropriate number of sodium ions[31] at random locations ensured electrical neutrality. The cut-off distance for the nonbonded interactions was 9 Å and periodic boundary conditions were used. Electrostatic interactions were treated by using the smooth particle mesh Ewald (PME) method[32] with a grid spacing of 1 Å. The SHAKE algorithm[33] was applied to all bonds involving hydrogen atoms and an integration step of 2.0 fs was used throughout. The molecular dynamics (MD) simulation protocol made use of sander (for the QM/MM part, see below) and pmemd modules in the AMBER 11 suite of programs.[34] Firstly, solvent molecules and counterions were relaxed by energy minimization and allowed to redistribute around the positionally restrained solute (25 kcal mol^{-1} Å^{-2}) during 50 ps of MD at constant temperature (300 K) and pressure (1 atm), essentially as described previously.[35] These initial harmonic restraints were gradually reduced in a series of progressive energy minimizations until they were completely removed. The resulting system, as well as those resulting from the hybrid QM/MM calculations described below, were heated from 100 to 300 K during 20 ps, equilibrated at 300 K for 1 ns and further simulated under the same conditions up to a total time of 10 ns during which system coordinates were collected every 20 ps for further analysis. NMR-type restraints were used during the initial classical MD for the Mg^{2+} coordinating sphere, that is, two water oxygen atoms, Oε(Glu79), OP1(Gua$_{15}$), and Oδ(Asn127) to avoid known problems of ligand exchange.[10] An additional restraint between one coordinating water oxygen and Oδ(Asn127) was also included but no restraints were applied between Mg^{2+} and O3′. The restraining values used were $r_1 = 1.30$, $r_2 = 1.80$, $r_3 = 2.19$, and $r_4 = 2.69$ Å with the force constants $k_2 = k_3 = 20$ kcal mol^{-1} Å^2. The final E–P simulation, which lasted 25 ns, was fully unrestrained. Each ns of MD took approximately 17 h of CPU time running in parallel on 32 IBM Power PC 970MP processors at the Barcelona Supercomputing Centre (MareNostrum).

Hybrid QM/MM calculations: Classical MM methods lack the ability to treat fundamentally quantum processes, such as bond breaking/forming and charge fluctuations as a function of geometry,[36] but it is possible to treat a subsection of the system by QM methods and use a coupling potential to connect the MM and QM regions. This hybrid QM/MM approach is seamlessly integrated in the sander module of AMBER 11[34] and also includes a complete treatment of long-range electrostatics by using a QM/MM modified PME method.[37,38] The QM region, defined by the iqmatoms keyword, encompassed the active site region where bonds are broken and formed, and the MM region included all the remaining protein, DNA and solvent atoms as well as the counterions. Care was taken not to cut any polar bonds when defining the QM/MM boundary. Thus, the QM region contained the whole of Ade$_{14}$ (up to C4′), the phosphate and C5′ of Gua$_{15}$, Mg^{2+} and its two coordinating water molecules, the catalytic water, and the side chains (starting from Cβ) of Glu79, His80, Trp78, Asn127 and Arg99. We selected the PM3 Hamiltonian[39] and full electrostatic interactions between the QM charge density (expanded in a STO-6G minimal basis set) and the point charges of the MM atoms. Three different reaction coordinates at constant velocities were implemented employing a steering MD protocol[40] and a linear combination of distances [Å] between pairs of atoms: 1) for activation of the water molecule by His80, attack of the resulting hydroxide onto the phosphorus atom and subsequent O3–P cleavage: $\xi = d_{OW-H} - d_{N-H}$ and $\xi = d_{PO3'} - d_{OWP}$; 2) for transfer of the proton from His80 to OP1: $\xi = d_{N-H} - d_{OP1-H}$, and 3) for proton transfer from OP2 to the O3′ leaving group: $\xi = d_{OP2-H} - d_{O3'-H}$. The time frames were 20 ps for (1), and 5 ps for (2) and (3) by using the recommended force constant of 1000 kcal mol^{-1} Å^{-2} in all cases. During the QM/MM part of the MD simulation SHAKE (keyword qmshake) was turned off and the integration step was reduced to 0.5 fs.

Analysis of the molecular dynamics trajectories: Three-dimensional structures and trajectories were visually inspected by using the computer graphics program PyMOL.[41] Interatomic distances and angles were monitored by using the ptraj module in AMBER and program Curves+.[42] Then 360° degrees were added to all negative torsion values for plotting purposes.

Normal mode analysis: The X-ray crystal structure of Vvn (PDB ID: 1OUO)[6] at 2.30 Å resolution was retrieved from the PDB.[2] An elastic network model connected all Cα atoms by springs representing the interatomic force fields and nonhydrogen protein atoms (within a cut-off of 10 Å) were considered as point masses. Vvn was then analyzed as a large set of coupled harmonic oscillators by using the NOMAD-Ref server[29] and default parameters. The ten lowest-frequency normal modes were calculated and each mode was explored in its two opposite directions. For the first nontrivial mode corresponding to the largest amplitude, the 30 resulting conformations were refined by geometry optimization of the side chains by using the sander module of AMBER 10.

Ligand docking: The CGRID and CDOCK programs,[43] as implemented in the VSDMIP platform,[44] were used to dock the minimal substrate deoxythymidine 3′,5′-bis-(*p*-nitrophenylphosphate) into the active site of Vvn, as found in PDB entry 1OUO.[6]

Acknowledgements

We are grateful to Dr. Alberto Gómez and Mr. Alvaro Cortés for assistance with VSDMIP and to Prof. María José Camarasa and Dr. Sonsoles Velázquez (IQM, CSIC) for many fruitful discussions. We thankfully acknowledge the generous allowance of computer resources, technical expertise and assistance provided by the Red Española de Supercomputación at the Barcelona Supercomputing Centre (MareNostrum). This work was partially supported by Comisión Interministerial de Ciencia y Tecnología (SAF2009-13914-C02-02) and Comunidad Autónoma de Madrid (S-BIO/0214/2006). J.A.B.-C. is a recipient of a research fellowship from PharmaMar S.A.U. (Colmenar Viejo, Madrid, Spain).

 © 2011 Wiley-VCH Verlag GmbH & Co. KGaA, Weinheim

Keywords: DNA cleavage · enzyme catalysis · molecular dynamics · quantum chemistry · water splitting

[1] E. S. Rangarajan, V. Shankar, *FEMS Microbiol. Rev.* **2001**, *25*, 583 – 613.
[2] F. C. Bernstein, T. F. Koetzle, G. J. Williams, E. F. Meyer, Jr., M. D. Brice, J. R. Rodgers, O. Kennard, T. Shimanouchi, M. Tasumi, *J. Mol. Biol.* **1977**, *112*, 535 – 542.
[3] S. V. Shlyapnikov, V. V. Lunin, M. Perbandt, K. M. Polyakov, V. Y. Lunin, V. M. Levdikov, C. Betzel, A. M. Mikhailov, *Acta Crystallogr. Sect. D* **2000**, *56*, 567 – 572.
[4] V. Y. Lunin, V. M. Levdikov, S. V. Shlyapnikov, E. V. Blagova, V. V. Lunin, K. S. Wilson, A. M. Mikhailov, *FEBS Lett.* **1997**, *412*, 217 – 222.
[5] M. Ghosh, G. Meiss, A. Pingoud, R. E. London, L. C. Pedersen, *J. Biol. Chem.* **2005**, *280*, 27990 – 27997.
[6] C. L. Li, L. I. Hor, Z. F. Chang, L. C. Tsai, W. Z. Yang, H. S. Yuan, *EMBO J.* **2003**, *22*, 4014 – 4025.
[7] Y. T. Wang, W. J. Yang, C. L. Li, L. G. Doudeva, H. S. Yuan, *Nucleic Acids Res.* **2007**, *35*, 584 – 594.
[8] C. M. Dupureur, *Metallomics* **2010**, *2*, 609 – 620.
[9] J. A. Cowan, *BioMetals* **2002**, *15*, 225 – 235.
[10] C. Chen, B. W. Beck, K. Krause, B. M. Pettitt, *Proteins Struct. Funct. Bioinf.* **2006**, *62*, 982 – 995.
[11] P. Friedhoff, G. Meiss, B. Kolmes, U. Pieper, O. Gimadutdinow, C. Urbanke, A. Pingoud, *Eur. J. Biochem.* **1996**, *241*, 572 – 580.
[12] M. D. Miller, J. Cai, K. L. Krause, *J. Mol. Biol.* **1999**, *288*, 975 – 987.
[13] B. Kolmes, I. Franke, P. Friedhoff, A. Pingoud, *FEBS Lett.* **1996**, *397*, 343 – 346.
[14] G. Meiss, O. Gimadutdinow, B. Haberland, A. Pingoud, *J. Mol. Biol.* **2000**, *297*, 521 – 534.
[15] K. C. Hsia, C. L. Li, H. S. Yuan, *Curr. Opin. Struct. Biol.* **2005**, *15*, 126 – 134.
[16] B. Loll, M. Gebhardt, E. Wahle, A. Meinhart, *Nucleic Acids Res.* **2009**, *37*, 7312 – 7320.
[17] E. A. Galburt, B. Chevalier, W. Tang, M. S. Jurica, K. E. Flick, R. J. Monnat, Jr., B. L. Stoddard, *Nat. Struct. Biol.* **1999**, *6*, 1096 – 1099.
[18] E. A. Galburt, B. L. Stoddard, *Biochemistry* **2002**, *41*, 13851 – 13860.
[19] K. E. Flick, M. S. Jurica, R. J. Monnat, Jr., B. L. Stoddard, *Nature* **1998**, *394*, 96 – 101.
[20] M. Midon, P. Schafer, A. Pingoud, M. Ghosh, A. F. Moon, M. J. Cuneo, R. E. London, G. Meiss, *Nucleic Acids Res.* **2011**, *39*, 623 – 634.
[21] E. Rico, J. F. Alzate, A. A. Arias, D. Moreno, J. Clos, F. Gago, I. Moreno, M. Dominguez, A. Jimenez-Ruiz, *Mol. Biochem. Parasitol.* **2009**, *163*, 28 – 38.
[22] P. Friedhoff, I. Franke, K. L. Krause, A. Pingoud, *FEBS Lett.* **1999**, *443*, 209 – 214.
[23] E. Marco, F. Gago, *ChemMedChem* **2007**, *2*, 1388 – 1401.
[24] A. Negri, E. Marco, J. Damborsky, F. Gago, *J. Mol. Graphics Modell.* **2007**, *26*, 643 – 651.
[25] A. Negri, D. Rodríguez-Larrea, E. Marco, A. Jiménez-Ruiz, J. M. Sánchez-Ruiz, F. Gago, *Proteins Struct. Funct. Bioinf.* **2010**, *78*, 36 – 51.
[26] K. Wang, M. Murcia, P. Constans, C. Perez, A. R. Ortiz, *J. Comput. Aided Mol. Des.* **2004**, *18*, 101 – 118.
[27] J. A. Cowan, *Chem. Rev.* **1998**, *98*, 1067 – 1088.
[28] K. A. Henzler-Wildman, V. Thai, M. Lei, M. Ott, M. Wolf-Watz, T. Fenn, E. Pozharski, M. A. Wilson, G. A. Petsko, M. Karplus, C. G. Hubner, D. Kern, *Nature* **2007**, *450*, 838 – 844.
[29] E. Lindahl, C. Azuara, P. Koehl, M. Delarue, *Nucleic Acids Res.* **2006**, *34*, W52 – W56.
[30] W. L. Jorgensen, J. Chandrasekhar, J. D. Madura, R. W. Impey, M. L. Klein, *J. Chem. Phys.* **1983**, *79*, 926 – 935.
[31] J. Aaqvist, *J. Phys. Chem.* **1990**, *94*, 8021 – 8024.
[32] T. A. Darden, D. York, L. Pedersen, *J. Chem. Phys.* **1993**, *98*, 10089 – 10092.
[33] J. P. Ryckaert, G. Ciccotti, H. J. C. Berendsen, *J. Comput. Phys.* **1977**, *23*, 327 – 341.
[34] D. A. Case, T. A. Darden, I. Cheatham, T. E., C. L. Simmerling, J. Wang, R. E. Duke, R. Luo, R. C. Walker, W. Zhang, K. M. Merz, B. Roberts, B. Wang, S. Hayik, A. Roitberg, G. Seabra, I. Kolossvai, K. F. Wong, F. Paesani, J. Vanicek, J. Liu, X. Wu, S. R. Brozell, T. Steinbrecher, H. Gohlke, Q. Cai, X. Ye, J. Wang, M.-J. Hsieh, G. Cui, D. R. Roe, D. H. Mathews, M. G. Seetin, C. Sagui, V. Babin, T. Luchko, S. Gusarov, A. Kovalenko, P. A. Kollman, University of California, San Francisco, **2010**, http://ambermd.org
[35] E. Marco, A. Negri, F. J. Luque, F. Gago, *Nucleic Acids Res.* **2005**, *33*, 6214 – 6224.
[36] G. M. de Seabra, R. C. Walker, M. Elstner, D. A. Case, A. E. Roitberg, *J. Phys. Chem. A* **2007**, *111*, 5655 – 5664.
[37] R. C. Walker, M. F. Crowley, D. A. Case, *J. Comput. Chem.* **2008**, *29*, 1019 – 1031.
[38] K. Nam, J. Gao, D. M. York, *J. Chem. Theory Comput.* **2004**, *1*, 2 – 13.
[39] J. J. P. Stewart, *J. Comput. Chem.* **1989**, *10*, 209 – 220.
[40] A. Crespo, M. A. Marti, D. A. Estrin, A. E. Roitberg, *J. Am. Chem. Soc.* **2005**, *127*, 6940 – 6941.
[41] W. D. Lano, DeLano Scientific LLC, **2006**, http://www.pymol.org/
[42] R. Lavery, M. Moakher, J. H. Maddocks, D. Petkeviciute, K. Zakrzewska, *Nucleic Acids Res.* **2009**, *37*, 5917 – 5929.
[43] C. Perez, A. R. Ortiz, *J. Med. Chem.* **2001**, *44*, 3768 – 3785.
[44] R. Gil-Redondo, J. Estrada, A. Morreale, F. Herranz, J. Sancho, A. R. Ortiz, *J. Comput. Aided Mol. Des.* **2009**, *23*, 171 – 184.

Received: July 31, 2011
Published online on October 6, 2011

 © 2011 Wiley-VCH Verlag GmbH & Co. KGaA, Weinheim